THE JOURNAL OF BIOLOGICAL CHEMISTRY VOL. 291, NO. 49, pp. 25667–25677, December 2, 2016

Structural Analysis of the Catalytic Mechanism and Substrate Specificity of *Anabaena* Alkaline Invertase InvA Reveals a Novel Glucosidase*

Received for publication, September 18, 2016, and in revised form, October 11, 2016 Published, JBC Papers in Press, October 24, 2016, DOI 10.1074/jbc.M116.759290

Jin Xie (谢进), Kun Cai (蔡坤), Hai-Xi Hu (胡海汐), Yong-Liang Jiang (江永亮), Feng Yang (杨丰), Peng-Fei Hu (胡鹏飞), Dong-Dong Cao (曹冬冬), Wei-Fang Li (李卫芳), Yuxing Chen (陈宇星)[1], and Cong-Zhao Zhou (周丛照)[2]

From the Hefei National Laboratory for Physical Sciences at the Microscale and School of Life Sciences, University of Science and Technology of China, Hefei Anhui 230027, China

Edited by Ruma Banerjee

Invertases catalyze the hydrolysis of sucrose to glucose and fructose, thereby playing a key role in primary metabolism and plant development. According to the optimum pH, invertases are classified into acid invertases (Ac-Invs) and alkaline/neutral invertases (A/N-Invs), which share no sequence homology. Compared with Ac-Invs that have been extensively studied, the structure and catalytic mechanism of A/N-Invs remain unknown. Here we report the crystal structures of *Anabaena* alkaline invertase InvA, which was proposed to be the ancestor of modern plant A/N-Invs. These structures are the first in the GH100 family. InvA exists as a hexamer in both crystal and solution. Each subunit consists of an $(\alpha/\alpha)_6$ barrel core structure in addition to an insertion of three helices. A couple of structures in complex with the substrate or products enabled us to assign the subsites −1 and +1 specifically binding glucose and fructose, respectively. Structural comparison combined with enzymatic assays indicated that Asp-188 and Glu-414 are putative catalytic residues. Further analysis of the substrate binding pocket demonstrated that InvA possesses a stringent substrate specificity toward the α1,2-glycosidic bond of sucrose. Together, we suggest that InvA and homologs represent a novel family of glucosidases.

Sucrose (α-D-glucopyranosyl-(1–2)-β-D-fructofuranose) is a major product of photosynthesis in plants and cyanobacteria and can be transported from the source tissues to heterotrophic sinks as a principal carbon carrier molecule (1). In the plant sink tissues sucrose is degraded into hexoses or derivatives to provide carbon and energy or to act as signaling molecules for the growth, development, and defense of plant (2–5). There are two enzymes that can cleave sucrose: sucrose synthase (SUS,[3] EC 2.4.1.13) and invertase (INV, EC 3.2.1.26) (1). SUS catalyzes the conversion of sucrose to fructose and UDP-glucose in a reversible manner, whereas INV irreversibly hydrolyzes sucrose into glucose and fructose. SUS-catalyzed sucrose cleavage is involved in the biosynthesis of storage and structural polysaccharides, such as starch and cellulose, and participates in modulating sink strength of plants (2, 6). In contrast, INV plays a central role in particular developmental stages (2, 7). For example, the activity of cytosolic INV but not SUS is required for the growth and reproduction of *Arabidopsis* (7).

Sucrose in cyanobacteria also plays an important role in environmental stress responses, glycogen metabolism, and nitrogen fixation as a carbon carrier molecule (8, 9). Recent studies implied that cyanobacteria utilize a similar set of enzymes as higher plants to metabolize sucrose; moreover, these enzymes seem to have a cyanobacterial origin (1, 4, 10). However, compared with the counterpart in higher plants, the mechanism of sucrose metabolism in cyanobacteria remains largely unclear (1, 10).

Invertases have been categorized into two major types according to their optimum pH values: acid invertases (Ac-Invs) with an optimum pH of 4.0–5.5, and alkaline/neutral invertases (A/N-Invs) with an optimum pH of 6.5–8.0 (11, 12). Usually A-Invs and N-Invs share a high sequence homology to each other and are often ambiguous but differ a lot from Ac-Invs. Ac-Invs can utilize sucrose and other β-fructose-containing oligosaccharides, such as raffinose and kestose, as the substrate and are, therefore, also termed β-fructofuranosidases (11). In contrast, it is generally accepted that A/N-Invs specifically catalyze the hydrolysis of sucrose (10, 11, 13). Ac-Invs are mainly localized in cell walls and vacuoles (14), whereas A/N-Invs are generally distributed in the cytosol and organelles, such as mitochondria and plastids (1). In addition, Ac-Invs are widespread in plants, fungi, and bacteria, whereas A/N-Invs have been only found in plants and photosynthetic bacteria (1, 10).

* This work was supported by National Natural Science Foundation of China Grants 31630001 and 31370757, 31621002, and 31500598 and Ministry of Education of China Grant 20133402110023. The authors declare that they have no conflicts of interest with the contents of this article.

The atomic coordinates and structure factors (codes 5GOO, 5GOP, 5GOQ, and 5GOR) have been deposited in the Protein Data Bank (http://wwpdb.org/).

[1] To whom correspondence may be addressed. Tel. and Fax: 86-551-63600406; E-mail: cyxing@ustc.edu.cn.

[2] To whom correspondence may be addressed. Tel. and Fax: 86-551-63600406; E-mail: zcz@ustc.edu.cn.

[3] The abbreviations used are: SUS, sucrose synthase; INV, invertase; Ac-Inv, acid invertase; A/N-Inv, alkaline/neutral invertase; GH, glycoside hydrolase; SeMet, selenomethionine; Suc, sucrose; r.m.s.d., root mean square deviation; tGA, a glucoamylase from *T. thermosaccharolyticum*; YgjK, a glucosidase from *E. coli*; SUH, a sucrose hydrolase from *X. axonopodis* pv. glycines; ELSD, evaporative light scattering detector; Bicine, *N*,*N*-bis(2-hydroxyethyl)glycine.

TABLE 1
Crystal parameters, data collection, and structure refinement

	SeInvA-Fru	SeInvA-Suc	SeInvA-Glc	Full-length InvA
Data collection				
Space group	$C222_1$	$C222_1$	$C222_1$	$P2_1$
Unit cell				
a, *b*, *c* (Å)	96.8, 177.9, 181.6	99.9, 178.9, 181.3	96.5, 179.1, 181.6	96.2, 179.3, 96.4
α, β, γ (°)				105.9
Resolution range (Å)	50.00-2.10 (2.18-2.10)[a]	50.00-2.35 (2.43-2.35)	50.00-2.75 (2.85-2.75)	50.00-2.67 (2.77-2.67)
Unique reflections	87,561 (8,440)	67,492 (6,760)	38,985 (3,895)	84,349 (8,478)
R_{merge}[b]	0.089 (0.535)	0.096 (0.512)	0.123 (0.525)	0.094 (0.430)
$I/\sigma I$	25.9 (3.8)	17.2 (2.9)	18.0 (2.8)	10.8 (3.1)
Completeness (%)	97.3 (95.0)	98.5 (99.7)	94.5 (96.1)	95.4 (97.0)
Average redundancy	6.3 (5.9)	3.8 (3.8)	8.8 (8.1)	2.9 (2.9)
Structure refinement				
Resolution range (Å)	31.79-2.11	33.96-2.35	48.90-2.75	30.50-2.67
R_{work}[c]/R_{free}[d]	0.193/0.218	0.207/0.235	0.187/0.233	0.192/0.235
Number of protein atoms	11,241	11,015	10,707	22,286
Number of water atoms	455	335	105	252
r.m.s.d.[e] bond lengths (Å)	0.005	0.004	0.007	0.010
r.m.s.d. bond angles (°)	1.041	1.084	1.096	0.976
Average B-factors (Å^2)				
Protein	35.0	30.0	48.0	64.0
Ligand	28.6, 40.9/24.3, 42.2/29.7, 43.6 (Fru, GOL)	29.2/20.8/32.4 (Suc/Fru/Suc)	41.5/38.0/42.7 (Glc)	59.1/60.8/62.5/60.7/58.4/63.0 (GOL)
Occupancy of ligand	1.00	0.90, 1.00, 0.88 (Suc/Fru/Suc)	1.00	1.00
Ramachandran plot[f] (residues, %)				
Most favored	98.27	97.93	98.46	97.80
Additional allowed	1.50	1.84	1.31	1.98
Outliers	0.23	0.23	0.23	0.22
MolProbity clash score[g]/score percentile	2.52/99th percentile (n = 557, 2.11 ± 0.25 Å)	3.07/100th percentile (n = 335, 2.35 ± 0.25 Å)	4.33/100th percentile (n = 200, 2.75 ± 0.25 Å)	3.66/100th percentile (n = 187, 2.67 ± 0.25 Å)
MolProbity score[h]/score percentile	1.04/100th percentile (n = 11356, 2.11 ± 0.25 Å)	1.11/100th percentile (n = 9377, 2.35 ± 0.25 Å)	1.21/100th percentile (n = 5926, 2.75 ± 0.25 Å)	1.20/100th percentile (n = 5381, 2.67 ± 0.25 Å)
Protein Data Bank entry	5GOO	5GOP	5GOQ	5GOR

[a] The values in parentheses refer to statistics in the highest bin.
[b] $R_{merge} = \sum hkl \sum_i |I_i(hkl) - \langle I(hkl)\rangle| / \sum_{hkl} \sum_i I_i(hkl)$, where $I_i(hkl)$ is the intensity of an observation, and $\langle I(hkl)\rangle$ is the mean value for its unique reflection. Summations are over all reflections.
[c] $R_{work} = \sum_h |F_o(h) - F_c(h)| / \sum_h F_o(h)$, where F_o and F_c are the observed and calculated structure factor amplitudes, respectively.
[d] R_{free} was calculated with 5% of the data excluded from the refinement.
[e] From ideal values.
[f] The categories were defined by Molprobity.
[g] The number of serious steric overlaps (>0.4 Å) per 1000 atoms.
[h] MolProbity score combines the clash score, rotamer, and Ramachandran evaluations into a single score, normalized to be on the same scale as X-ray resolution.

Ac-Invs, which belong to glycoside hydrolase 32 (GH32) family, share an all-β structure with the active sites located at a 5-fold β-propeller domain and adopt double displacement mechanism for hydrolysis (15–18). Recently, emerging evidence implies that A/N-Invs play key roles in cell growth (7, 13, 19, 20), reproductive development (20, 21), and oxidative stress defense (22). Bioinformatics analysis revealed that most genome-sequenced cyanobacteria encode only A/N-Invs but not Ac-Invs. Vargas *et al.* (10) identified two A/N-Invs from the filamentous nitrogen-fixing cyanobacterium *Anabaena* sp. PCC 7120, which represents the alkaline and neutral invertase, namely InvA and InvB, respectively. Moreover, InvA is only expressed in vegetative cells, and its invertase activity can be inhibited by fructose like other A/N-Invs (9, 10). In contrast to well investigated Ac-Invs, the structure and catalytic mechanism of A/N-Invs remain unknown.

Here, we report the crystal structures of *Anabaena* InvA and its complexes with the substrate or product, which represent the first structure of A/N-Invs and the first member of known structures in GH100 family. InvA adopts an overall structure of $(\alpha/\alpha)_6$ barrel that completely differs from Ac-Invs. Structural analyses combined with activity assays reveal a well defined active-site pocket, which determines the stringent substrate specificity toward the α1,2-glycosidic bond of sucrose. In addition, we assigned active-site residues, which enabled us to propose a putative catalytic mechanism of InvA. The distinct structure and catalytic mechanism indicate that InvA and its homologous A/N-Invs belong to a novel family of glucosidases but not the previously reported β-fructofuranosidases (23, 24).

Results

Overall Structure of InvA—We obtained crystals of the full-length InvA (NCBI accession number WP_010995690.1, residues Met-1–Leu-468) at 2.67 Å resolution but failed in optimizing the selenomethionine (SeMet)-substituted crystals for phase determination. Partial proteolysis and multiple sequence alignment indicated that both N and C termini are somewhat unstructured. Thus, we overexpressed and purified a truncated version of InvA (residues Lys-9–Thr-460) and successfully optimized its crystal co-crystallized with 200 mM fructose, the 2.11 Å SeMet-substituted crystal of which was used for structure determination. In fact, we have not observed crystals of InvA in the absence of fructose, which was proposed to be an inhibitor of InvA (10). Eventually, we obtained the glucose and sucrose-complexed crystals by soaking crystals of truncated InvA with glucose and sucrose, respectively. The full-length InvA structure and the complex structures of truncated InvA with sucrose and glucose were solved by using the fructose co-crystallized structure (InvA-Fru) as the initial model. The parameters for data collection and structure determination of all structures are listed in Table 1.

In the sucrose-complexed structure (InvA-Suc), which has a space group of $C222_1$, each asymmetric unit contains three molecules of InvA. Symmetry operation and assembly analysis

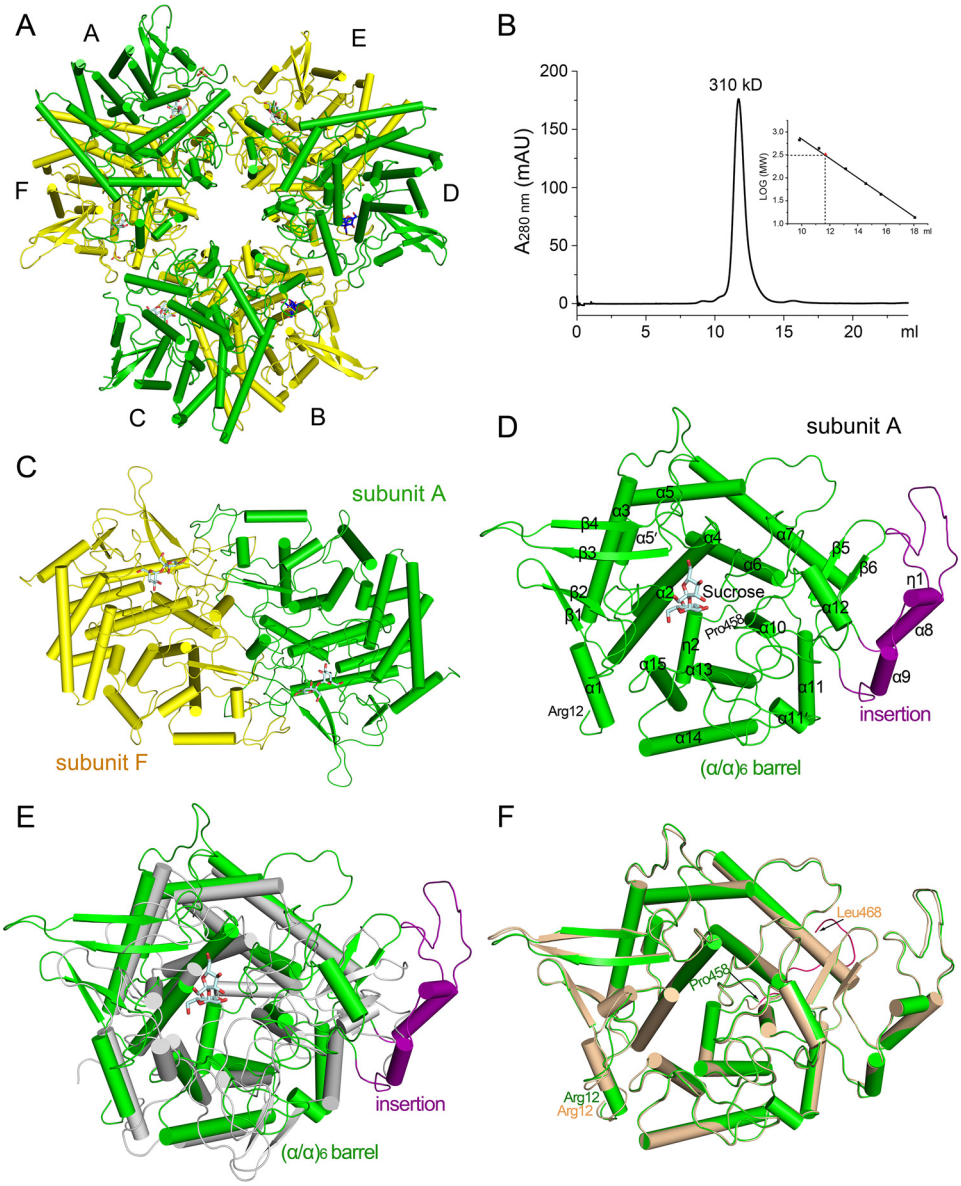

FIGURE 1. **Overall structure of InvA.** *A*, hexameric structure. Helices are shown as *cylinders*; sucrose and fructose in the active site are shown as *pale cyan* and *blue sticks*, respectively. Two subunits in each dimer are colored in *green* and *yellow*, respectively. The six subunits are sequentially labeled as *A–F*. *B*, molecular mass determination of InvA by analytical gel filtration chromatography. *mAU*, milliabsorbance units. *C*, dimeric structure. A dimer of subunits A and F is shown. *D*, a close view of InvA monomer. Subunit A in InvA-Suc is used as an example. The core $(\alpha/\alpha)_6$-barrel is shown in *green*, and the insertion is colored in *purple*. The sucrose molecule is shown in sticks. *E*, superposition of InvA against the catalytic domain of tGA, which is shown in *gray*. *F*, superposition of truncated InvA (InvA-Suc) against the full-length structure. InvA-Suc and the full-length structure are shown in *green* and *wheat*, respectively. A loop at the C terminus of the full-length structure is highlighted in *hot pink*.

using PDBePISA (25) revealed that InvA forms a hexamer (Fig. 1*A*). Notably, each asymmetric unit of the full-length InvA structure in a space group of $P2_1$ has six subunits, which also form a hexamer. In fact, InvA exists as hexamer in solution as well as shown in the gel-filtration profile (Fig. 1*B*). Further analysis of the dimeric and trimeric interfaces using PDBePISA indicated that the hexamer displays a trimer of dimers (Fig. 1*C*). The two subunits of each dimer have a total buried interface of ~6400 Å^2, whereas the two neighboring dimers have an interface of ~2300 Å^2.

Taking the InvA-Suc structure as an example, the three subunits in each asymmetric unit share an overall structure very similar to each other, with a root mean square deviation (r.m.s.d.) of 0.40–0.53 Å over 436 Cα atoms. As residues Arg-12–Pro-458 could be clearly traced in the electron density map of subunit A, we take it as an example for further structure analysis. The DALI search (26) revealed that InvA has a very high structural homology to $(\alpha/\alpha)_6$-barrel glycoside hydrolases (GHs) and several phosphorylases. The catalytic domain of a glucoamylase from *Thermoanaerobacterium thermosaccharolyticum*, termed tGA (27), has the highest Z score in the output of GHs (PDB entry 1LF6, Z score 30.2, r.m.s.d. 3.1 Å over 330 residues, sequence identity 14%). Similar to the catalytic domains of tGA, InvA monomer consists of an $(\alpha/\alpha)_6$-barrel core structure (Fig. 1*D*). However, superposition of two structures revealed that InvA possesses an insertion of three helices beyond the core structure (Fig. 1*E*). Notably, InvA significantly differs from the Ac-Invs, which share an all-β structure (15).

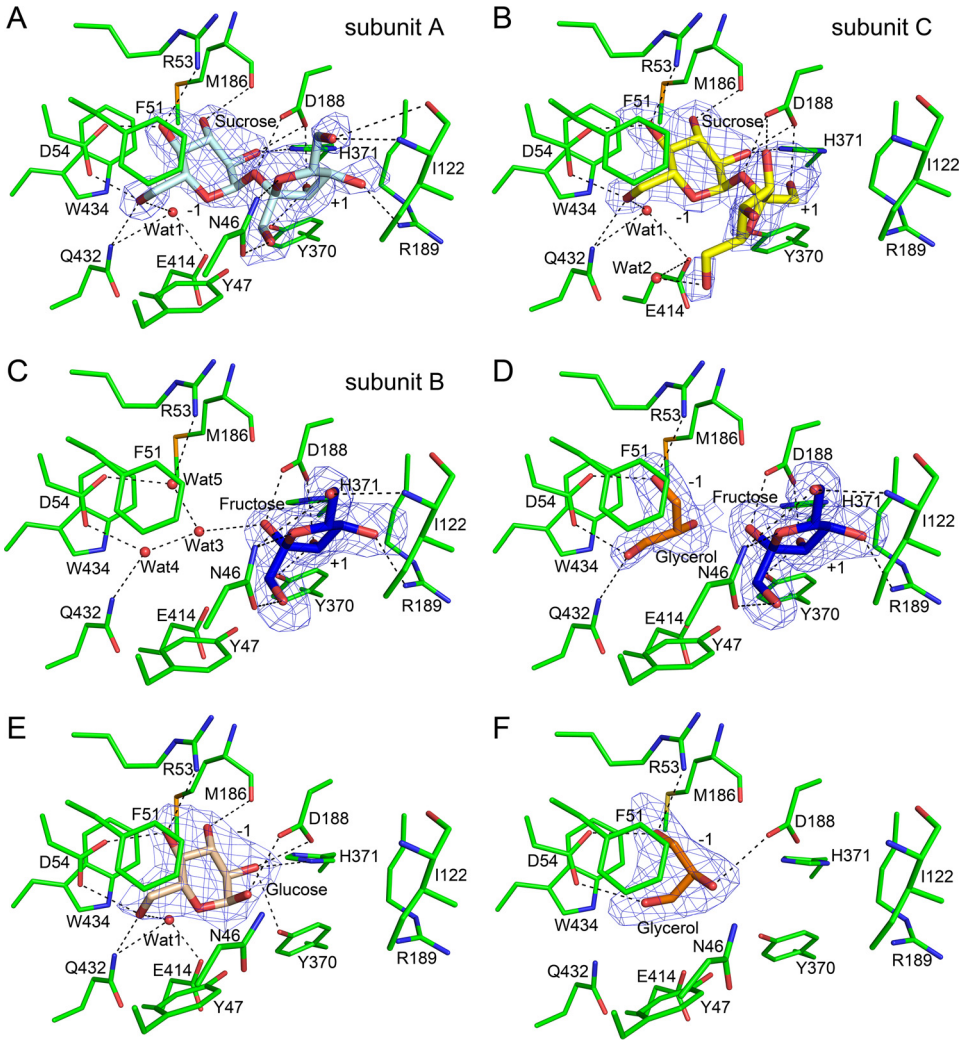

FIGURE 2. **The substrate binding pocket of InvA.** Shown are the small molecules binding to the pocket of subunit A (*A*), subunit C (*B*), and subunit B (*C*) of the sucrose-complexed structure InvA-Suc. *D*, fructose binding to the subsite +1 in the fructose-complexed structure InvA-Fru. *E*, glucose at the subsite −1 in the glucose-complexed structure InvA-Glc. *F*, glycerol at the subsite −1 in the full-length structure of InvA. The involved residues are shown in *green sticks*, the ligands are shown as sticks in different colors, and the water molecules are shown as *red spheres*. The polar interactions are indicated by *dashed lines*. The simulated annealing $F_o - F_c$ difference electron density maps of ligands contoured at 3.0 σ are shown as *blue mesh*.

In detail, the core $(\alpha/\alpha)_6$ barrel structure of InvA is mainly composed of 12 α-helices, which are arranged in two concentric layers in a way similar to that of glycoside hydrolases in the clans GH-G, GH-L ,and GH-M (27–32). The 12 α-helices form six helical hairpins, five of which are connected via a short loop, except for α1/α15. The neighboring helical hairpins are further linked by longer interhairpin loops, which are proposed to form the catalytic pocket and oligomeric interface. Compared with structure-known $(\alpha/\alpha)_6$-barrel glycoside hydrolases, the major difference comes from an insertion (residues Asp-246–Gly-288) composed of helices α8, α9, and η1. The insertion contributes to the majority of the interdimer interactions, which enable the formation of InvA hexamer. Notably, the full-length structure of InvA shares an overall structure almost identical to that of the three truncated complexes, with an r.m.s.d. ranging from 0.25 to 0.53 Å over 437 Cα atoms except for a loop of the most C-terminal 10 residues from Asp-459 to Leu-468 (Fig. 1*F*).

The Active-site Pocket—In the sucrose-complexed structure InvA-Suc, the three subunits of each asymmetric unit bind three types of small molecules. Subunits A and C accommodate a sucrose molecule in each putative catalytic pocket; however, the two sucrose molecules adopt different conformations in terms of the orientation of the fructosyl moiety (Fig. 2, *A* and *B*). Surprisingly, subunit B binds to a fructose molecule (Fig. 2*C*), which was most likely incorporated during crystallization. The sucrose molecules in subunits A and C are stabilized by a cluster of interhairpin loops. In both subunits the glucosyl moiety is locked at the inner part (subsite −1) of the pocket by hydrogen bonds with Arg-53, Asp-54, Met-186, Asp-188, His-371, Gln-432, and the water molecule Wat1 (Fig. 2, *A* and *B*). Remarkably, the two side-chain oxygen atoms of Asp-54 act as a pair of tweezers to anchor the glucose ring via two hydrogen bonds with O4 and O6 atoms in a way similar to that of YgjK and tGA (27, 28). In subunit A, the fructosyl moiety binds to Asn-46, Ile-122, Asp-188, Arg-189, and Tyr-370 at subsite +1 via polar interactions (Fig. 2*A*). In contrast, the fructosyl moiety in subunit C has less contact with the subsite +1 via only three hydrogen bonds with the side chain of Asp-188 and one water molecule (Fig. 2*B*). In addition, hydrophobic interactions from the aromatic residues, such as Phe-51, Tyr-370, and Trp-434, also

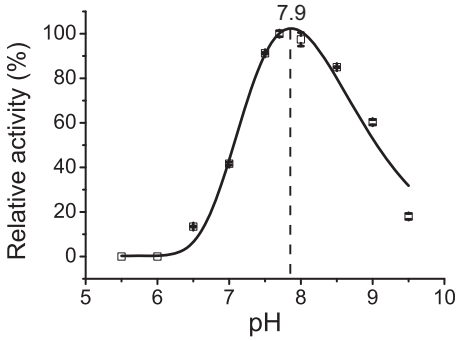

FIGURE 3. **The optimum pH of InvA.** Invertase activity was measured against 100 mM sucrose at pH 5.5–9.5. Three independent experiments were performed, and the S.D. of the mean are shown as *error bars*.

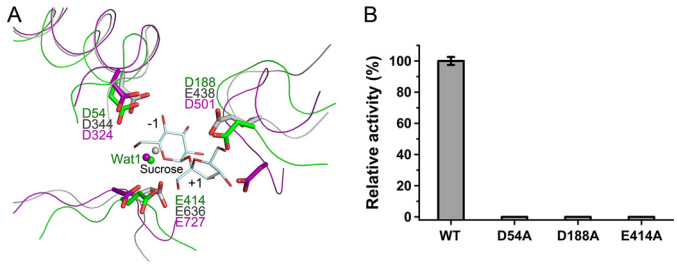

FIGURE 4. **Catalytic residues of InvA.** *A*, superposition of the active sites of InvA, tGA, and YgjK. The corresponding secondary elements and residues of InvA, tGA, and YgjK are shown in *green*, *gray*, and *purple*, respectively. The catalytic water molecule is displayed as a *sphere* in a corresponding color. *B*, the relative activity of the three mutants compared with the wild-type InvA. The *error bars* represent S.D. from three independent assays.

contribute to stabilizing the sucrose molecule in both subunits. It is worthwhile to mention that in subunit C residues from Leu-42 to Asp-48 in the loop between β2 and α2 are missing in the electron density map.

Different from subunits A and C, subunit B of InvA-Suc binds a fructose molecule at the subsite +1 (Fig. 2*C*). This fructose molecule adopts a conformation and binding pattern identical to that in the fructose co-crystallized structure InvA-Fru (Fig. 2*D*). Moreover, both the two fructose molecules from InvA-Suc and InvA-Fru could be well superimposed against the fructosyl moiety of the sucrose at subsite +1 in subunit A of InvA-Suc.

In addition, we also solved the structure of InvA in complex with another product, glucose, termed InvA-Glc. Similar to that of the glucosyl moiety of sucrose in InvA-Suc structure, the glucose molecule occupies subsite −1 in an almost identical binding pattern (Fig. 2*E*). Notably, we tried extensively to obtain the apo-form structure of InvA; however, only the full-length InvA yielded crystals of a relatively low resolution (2.67 Å). Nevertheless, a glycerol molecule, which was used as the cryoprotectant, occupies the subsite −1 (Fig. 2*F*).

Taken together, we obtained six structures of the substrate binding pocket, which is occupied by various molecules. Structural comparisons revealed that the subsites −1 and +1 are stringently selective toward glucose and fructose, respectively.

The Enzymatic Properties and Catalytic Residues—To further explore the catalytic mechanism of InvA, we first performed a series of assays to determine its enzymatic parameters. Our purified InvA possesses the highest activity at an optimum pH of 7.9 (Fig. 3), which is similar to the optimum pH determined by Vargas *et al.* (10). In addition, we detected that InvA has a Michaelis constant (K_m) toward sucrose of 20.8 ± 1.7 mM, comparable to the plant A/N-Invs in a range of 8–30 mM (13, 22, 33–36) but higher than that of Ac-Invs at 0.5–10 mM (37–41). Furthermore, we determined that InvA has a turnover number (k_{cat}) of 73.7 ± 1.9 s^{-1}, at the same level as or somewhat lower than several previously reported Ac-Invs (37, 40, 42, 43). Thus in general InvA has a lower activity compared with Ac-Invs. Despite that InvA exists as a hexamer in both crystal and solution, a Hill coefficient (n_H) of 0.88 ± 0.08 indicates no cooperativity among the subunits. Notably, most plant A/N-Invs also assemble into oligomers, either tetramers (23, 34, 44, 45) or octamers (24).

To assign the catalytic residues of InvA, we performed a comparative structural analysis against its structural homologs tGA (Fig. 1*E*) and *Escherichia coli* glucosidase YgjK (PDB entry 3W7S, Z score 28.6, r.m.s.d. 3.2 Å for 343 residues). Despite sharing only a sequence identity of about 14 and 11%, respectively, to tGA and YgjK, InvA also consists of a very similar $(\alpha/\alpha)_6$-barrel catalytic domain (Fig. 1*E*). Previous reports proposed that tGA and YgjK adopt a general acid-base mechanism to hydrolyze the glycosidic bond using Glu-438 and Glu-636 of tGA or Asp-501 and Glu-727 of YgjK (27, 28). Structural superposition clearly indicated that residues Asp-188 and Glu-414 of InvA, in addition to Wat1 and the corresponding loops that harbor these two acidic residues, could be well superimposed against the catalytic residues and the nucleophilic water molecule of both tGA and YgjK (Fig. 4*A*). Moreover, the side chain of Asp-54 of InvA, which locks the glucosyl moiety at subsite −1, also adopts a same conformation as the major sugar binding residue, Asp-344 of tGA or Asp-324 of YgjK (Fig. 4*A*). To validate the crucial role of these residues in catalysis, we prepared their single mutants. As predicted, no mutants exhibited detectable activity toward sucrose (Fig. 4*B*). Therefore, we propose that InvA utilizes Asp-188 and Glu-414 as the catalytic residues and adopts the general acid-base mechanism (Fig. 5) similar to that of tGA and YgjK. The hydrolysis is triggered by the nucleophilic attack of the water molecule Wat1 toward the anomeric carbon atom of glucosyl moiety. The catalytic base, Glu-414, assists hydrolysis by abstracting a proton from Wat1, whereas the catalytic acid, Asp-188, which is on the opposite side, donates a proton to the target oxygen atom, resulting in cleavage of the glycosidic bond.

Stringent Substrate Specificity—Despite the two types of invertases are capable of hydrolyzing sucrose, A/N-Invs are distinct from Ac-Invs from many points of view. Ac-Invs have been classified into the β-fructofuranosidases, as they are able to catalyze the release of β-fructose from the non-reducing end of various β-fructofuranoside substrates besides sucrose (11, 37). Crystal structures demonstrated that the subsite −1 of Ac-Invs specifically recognizes the fructose ring of a given substrate that lies in a rather open pocket, resulting in a broad spectrum of substrates (15). However, the reports concerning the substrate specificity of A/N-Invs are controversial, either specifically hydrolyzing sucrose (10, 11, 13, 33) or also possessing hydrolytic activity toward some β-fructose-containing sugars such as raffinose and stachyose or maltose in addition to

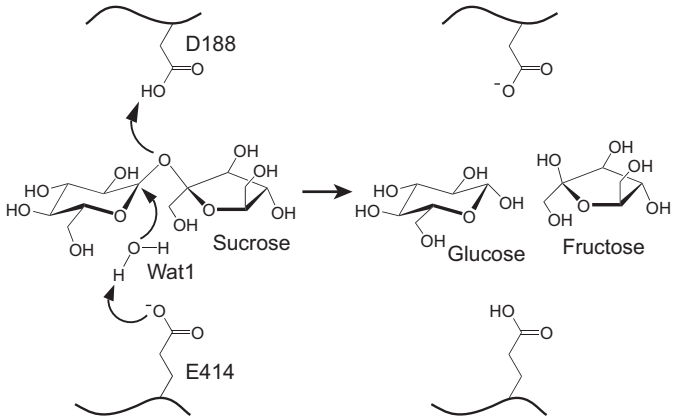

FIGURE 5. **A putative catalytic mechanism of InvA.** Residues Asp-188 and Glu-414 are proposed to be the catalytic acid and base, respectively. Wat1 is the presumed nucleophilic water molecule.

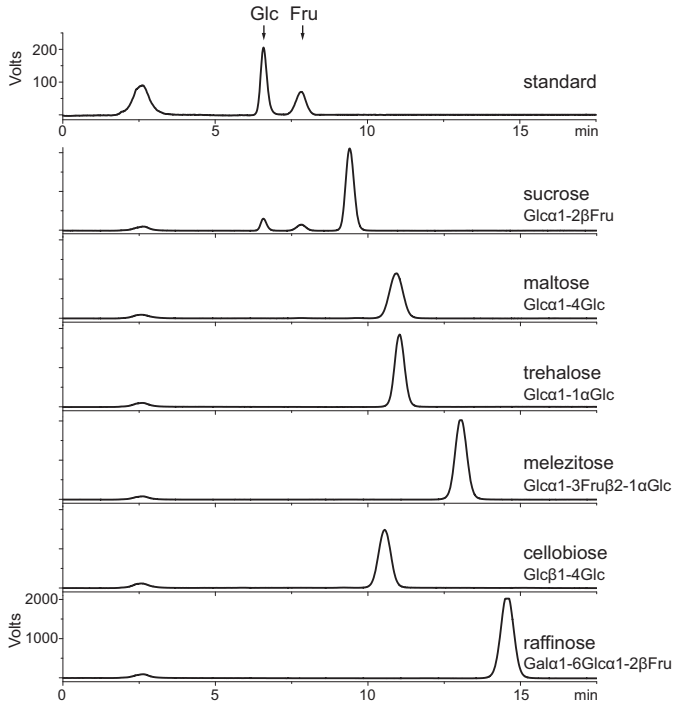

FIGURE 6. **The substrate specificity of InvA.** HPLC analysis of the hydrolytic activity of InvA toward 100 mM various sugars. The *upper panel* is the standard sample of glucose and fructose. The formulas of tested sugars are shown on the *right of the corresponding profiles*.

sucrose, albeit at a lower rate (23, 24, 45, 46). As shown in our structures (Fig. 2, *A* and *B*), InvA adopts a rather closed substrate binding pocket that is perfectly complementary to a sucrose molecule, different from an open catalytic pocket of Ac-Invs. Moreover, the glucosyl moiety is located at the subsite −1 of the substrate binding pocket of InvA (Fig. 2, *A* and *B*), and the hydrolysis happens to the α1,2 glycosidic bond.

To further explore the substrate specificity of InvA in solution, we tested its hydrolytic activity toward various sugars: oligosaccharides with an α-D-glucopyranosyl moiety at the non-reducing end, such as maltose (Glcα1–4Glc), trehalose (Glcα1–1αGlc), and melezitose (Glcα1–3Fruβ2–1αGlc) in addition to cellobiose (Glcβ1–4Glc), which has a non-reducing β-D-glucose. We also checked the activity of InvA toward raffinose (Galα1–6Glcα1–2βFru), a typical substrate of β-fructofuranosidases. The results suggested that InvA only catalyzes the hydrolysis of sucrose but not any other selected sugars (Fig. 6). Notably, the trisaccharide melezitose, which has a sucrose moiety with exposed glucosyl residue, could not be hydrolyzed by InvA. Thus, we demonstrated that InvA is stringently specific toward sucrose, in agreement with the previous report (10). Multiple sequence alignment indicated that the catalytic and substrate binding residues are strictly conserved among all A/N-Invs ranging from cyanobacteria and photosynthetic bacteria to plants (Fig. 7). We, therefore, hypothesize that InvA and its homologs share a similar substrate binding pattern and catalytic mechanism. The previous controversies concerning the activity of A/N-Invs are most likely due to contamination during purification of the native enzymes (33).

Discussion

A/N-Invs Represent a Novel Family of Glucosidases—Our results demonstrated that InvA, very likely as well as other A/N-Invs, specifically catalyzes the hydrolysis of the α1,2-glycosidic bond in sucrose. A/N-Invs have been exclusively classified into an individual glycoside hydrolase family, termed GH100, in the carbohydrate active enZyme (CAZy) database (47). However, as proposed by the Nomenclature Committee of the International Union of Biochemistry and Molecular Biology (Enzyme Nomenclature), they are categorized into β-fructofuranosidases of EC 3.2.1.26 together with Ac-Invs. Homology search using BLAST (blast.ncbi.nlm.nih.gov) revealed that InvA shows the highest similarity to amylo-α-1,6-glucosidase (EC 3.2.1.33) at a sequence identity of 21%. However, amylo-α-1,6-glucosidase catalyzes the hydrolysis of an α1,6 but not an α1,2-glycosidic bond. The current glycoside hydrolases that catalyze α1,2-glycosidic bonds with the non-reducing α-glucose deposited in BRENDA database (48) include sucrose α-glucosidase/sucrase (EC 3.2.1.48), mannosyl-oligosaccharide glucosidase (EC 3.2.1.106), glucosyl-galactosyl-hydroxylysine glucosidase (EC 3.2.1.107), and branched-dextran exo-1,2-α-glucosidase (EC 3.2.1.115) (Table 2). However, they all display a different substrate specificity (49–53) compared with InvA. Although sucrases, which are widespread in animals, are able to hydrolyze sucrose, they also recognize some longer α1,2-linked oligosaccharides and cleavage α1,4-glycosidic bonds of terminal starch or glycogen digestion products (49, 50). Remarkably, a *Xanthomonas axonopodis* sucrase termed SUH that belongs to GH13 family has been shown to catalyze only sucrose among a limited list of selected sugars (54). However, SUH has a different catalytic domain of $(\beta/\alpha)_8$ barrel and a much longer substrate binding pocket that could accommodate a oligosaccharide substrate much longer than the sucrose (55). Together, InvA and homologous A/N-Invs represent a novel family of glucosidases, which only specifically catalyze the cleavage of α1,2-glycosidic bond of sucrose.

In summary, we have solved the first structure of A/N-Invs, which are distinct from Ac-Invs. Identification of the catalytic residues enabled us to demonstrate that InvA possesses a stringent substrate specificity toward sucrose. These findings not only clarify the classification of A/N-Invs but also provide clues

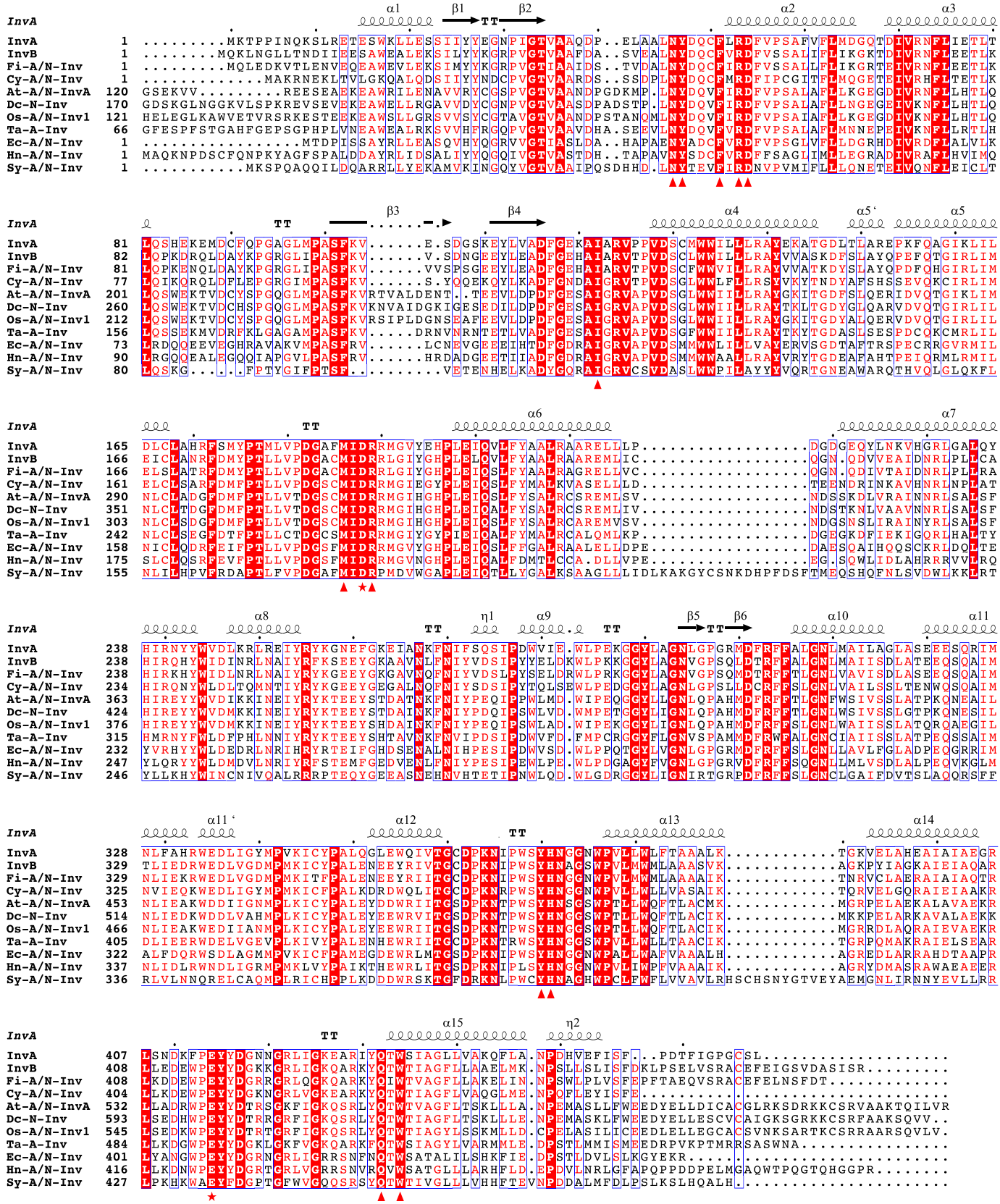

FIGURE 7. **Multiple sequence alignment of InvA and homologous A/N-Invs.** Secondary structure elements of InvA are shown at the top of alignment. The catalytic residues and substrate binding residues are depicted by *red stars* and *red triangles*, respectively. The sequences of InvA and homologs are from the following organisms: *Anabaena* sp. PCC 7120 (InvA, WP_010995690.1; InvB, CAC85155.1), *Fischerella* sp. JSC-11 (Fi-A/N-Inv, ZP_08987807.1), *Cyanothece* sp. PCC 7822 (Cy-A/N-Inv, WP_013325329.1), *Arabidopsis thaliana* (At-A/N-InvA, NP_176049.1), *Daucus carota* (Dc-N-Inv, CAA76145.1), *Oryza sativa* subsp. Japonica (Os-A/N-Inv1, NP_001049936), *Triticum aestivum* (Ta-A-Inv, CAL26914.1), *Ectothiorhodospira* sp. PHS-1 (Ec-A/N-Inv, ZP_09695138.1), *Halothiobacillus neapolitanus* c2 (Hn-A/N-Inv, WP_012823125.1), and *Synechocystis* sp. PCC 6803 (Sy-A/N-Inv, CAD33848.1).

TABLE 2
Invertases and glycoside hydrolases that catalyze α1,2-glycosidic bonds with a non-reducing α-glucose

Enzyme	EC number	Substrates	Glycosidic bonds	GH families	Structures
A/N-Inv		Sucrose	α1,2-Linkage	100	$(\alpha/\alpha)_6$ Barrel
β-Fructofuranosidase	3.2.1.26	Sucrose and other β-D-fructofuranosides	Terminal non-reducing β-D-fructofuranoside residues	32, 68	5-Fold β-propeller
Sucrose α-glucosidase/sucrase	3.2.1.48	Terminal starch/glycogen digestion products and α1, 2-linked oligosaccharides	Linkages of α1,2 (sucrase subunit), α1,6/α1,1 (isomaltase subunit), α1,4 (both)	13, 31	$(\beta/\alpha)_8$ Barrel
Mannosyl-oligosaccharide glucosidase	3.2.1.106	$Glc_3Man_9GlcNAc_2$	Terminal α1,2-linkage	63	$(\alpha/\alpha)_6$ Barrel
Glucosyl-galactosyl-hydroxylysine glucosidase	3.2.1.107	α-D-Glucosyl-1,2-β-D-galactosyl-L-hydroxylysine	α1,2-linkage	65	$(\alpha/\alpha)_6$ Barrel[a]
Branched-dextran exo-1,2-α-glucosidase	3.2.1.115	Branch points of dextrans and related polysaccharides	α1,2-Linkage		

[a] Structures of members in GH65 but not a member in EC 3.2.1.107.

to further investigation of sucrose metabolism in cyanobacteria and plants.

Experimental Procedures

Cloning, Expression, and Purification—The gene of InvA (NCBI accession number WP_010995690.1, 468 residues) was amplified from the genomic DNA of *Anabaena* sp. PCC 7120. The full-length *invA* and mutants were cloned into a modified pET28a vector with an N-terminal His_6 tag. Likewise, the truncated InvA covering residues Lys-9–Thr-460 was constructed for crystallization. Both the wild-type and mutant proteins were overexpressed in *E. coli* strain BL21 (DE3) (Novagen). The bacteria were grown in LB culture medium (10 g of Tryptone, 5 g of yeast extract, and 10 g of NaCl per liter) containing 30 μg/ml kanamycin at 37 °C to the $A_{600\ nm}$ of 0.6. Then protein expression was induced with 0.2 mM isopropyl β-D-1-thiogalactopyranoside at 37 °C for 4 h. Cells were collected and resuspended in the lysis buffer (20 mM HEPES, pH 8.0, 100 mM NaCl). After 12 min of sonication and centrifugation at 12,000 × *g* for 25 min, the supernatant containing the target protein was loaded onto a nickel-nitrilotriacetic acid column (Qiagen) equilibrated with the binding buffer (20 mM HEPES, pH 8.0, 100 mM NaCl). The target protein was eluted with 300 mM imidazole and further loaded onto a HiLoad 16/600 Superdex 200 pg column (GE Healthcare) equilibrated with the binding buffer. Fractions containing the target protein were combined and concentrated to 5–10 mg/ml for crystallization. Samples for enzymatic activity assays were collected at the highest peak fractions without concentration and stored at −80 °C with 50% glycerol. The purity of protein was assessed by gel electrophoresis.

Analytical gel filtration chromatography was used to determine the molecular weight of InvA in solution by a Superdex 75 10/300 GL column (GE Healthcare). The following standard molecular markers were used for calibration: ribonuclease A (13.7 kDa), ovalbumin (43.0 kDa), conalbumin (75.0 kDa), aldolase (158.0 kDa), ferritin (440.0 kDa), and thyroglobulin (669.0 kDa).

SeMet-substituted full-length and truncated InvA were overexpressed in *E. coli* B834 (DE3) (Novagen). Transformed cells were first cultured in LB medium at 37 °C overnight, then harvested and washed twice with the M9 medium (56). Then the cells were cultured in SeMet medium (M9 medium with 50 mg/liter SeMet and other essential amino acids at 50 mg/liter) to an $A_{600\ nm}$ of 0.6–0.8. The following steps in protein expression and purification were the same as those for the native protein in addition to adding 5 mM β-mercaptoethanol during purification.

Crystallization, Data Collection, and Processing—Crystals were grown using the hanging drop vapor diffusion method, with a drop of 1 or 2 μl of protein solution mixed with an equal volume of reservoir solution. Microseeding was adopted in crystal optimization. Crystals of the full-length InvA were grown at 14 °C, whereas crystals of the truncated version were first grown at 14 °C for 2 days and then transferred to 25 °C for ~1 week. Crystals were obtained against the reservoir solution of 27% polyethylene glycol 6000, 0.1 M Bicine, pH 9.0, for the native and SeMet-substituted full-length protein and 1.5 M Li_2SO_4 and 0.1 M Tris, pH 8.5, for the SeMet-substituted trun-

cated InvA. In addition, a protein solution of the SeMet-substituted truncated InvA was incubated with 200 mM fructose before crystallization. Crystals were transferred to cryoprotectant (reservoir solution supplemented with 30% glycerol) and flash-cooled with liquid nitrogen. For soaking experiments, the fructose-complexed crystals were transferred to 2 μl of mother liquor containing 30% saturated sucrose (~1.8 M) and glucose (~1.5 M). Fructose might be competitively dissociated during soaking with sucrose or glucose. After 5 min, crystals soaking with sucrose were flash-cooled directly with sucrose as the cryoprotectant, whereas 30% glycerol was used as the cryoprotectant for the glucose soaked crystals.

X-ray diffraction data were collected at 100 K in a liquid nitrogen stream using beamline BL17U with an ADSC Q315r CCD detector and beamline BL18U with a DECTRIS PILATUS 6M PIXEL detector at the Shanghai Synchrotron Radiation Facility (SSRF). All diffraction data were integrated and scaled with the program HKL2000 (57).

Structure Determination and Refinement—The crystal structure of SeMet-substituted InvA in complex with fructose was determined by the single-wavelength anomalous dispersion method (58) using the anomalous signal of Se. The AutoSol program of PHENIX (59) was used to search the heavy atoms and calculate the phase. In total 35 selenium sites were identified among all 39 sites in the asymmetric unit. Then automatic model building was carried out using Autobuild in PHENIX. The resultant model contains 1260 residues (93% completeness) with R_{work} and R_{free} values of 0.195 and 0.222, respectively. The initial model was refined using the maximum likelihood method implemented in REFMAC5 (60) of CCP4i program suite (61) and rebuilt interactively using the program COOT (62). The InvA-Fru structure was used as the search model against the crystal data of full-length InvA by molecular replacement using Molrep program (63) in CCP4i. The InvA-Suc and InvA-Glc data were refined against the InvA-Fru structure. Subsequent refinements were performed by REFMAC5 program in CCP4i, phenix.refine program (64), in PHENIX and COOT. Non-crystallographic symmetry restraints were used during refinements of the full-length InvA and InvA-Glc structures, which have modest resolutions. The final model was evaluated with the web service MolProbity (65). Crystallographic parameters were listed in Table 1. The simulated annealing $F_o - F_c$ difference maps of different ligands contoured at 3.0 σ were calculated by PHENIX. The oligomeric state and interface areas were calculated by PDBePISA. All structure figures were prepared with PyMOL.

Enzymatic Assays—The pH dependence of invertase activity of recombinant InvA was assayed in 40 mM MES (pH 5.5–6.5), HEPES (pH 7.0–8.0), Bicine (pH 8.5–9.0), and glycine-NaOH (pH 9.5) buffer containing 100 mM NaCl. Subsequent enzymatic assays were carried out at pH 7.9. A 50-μl reaction mixture containing 100 mM sucrose and 50 nM wild-type enzyme or the mutants was incubated at 30 °C for different time courses. Then the reactions were stopped by heating at 95 °C for 10 min. After centrifuged at 12,000 × *g* for 10 min, the supernatant was diluted 10-fold and analyzed by HPLC system (Agilent 1200 Series) coupled with an evaporative light scattering detector (ELSD, Alltech 2000ES). An acetonitrile/water (70:30, v/v) solution was used as the mobile phase at 1 ml/min. The samples were injected in volumes of 10 μl onto a Prevail^{TM} Carbohydrate ES column (4.6 × 250 mm, 5 μm, GRACE), and the column temperature was kept at 25 °C. For ELSD, the temperature of the nebulizer was set to 85 °C, and the gas flow was 2.5 liter/min. The glucose standards were used to construct the calibration curve for quantification each time. The kinetic determinations of wild-type InvA were performed at different sucrose concentrations, and the K_m and k_{cat} values were calculated by nonlinear fitting to the Michaelis-Menten equation using the program Origin 8. The n_H value was calculated by the Hill equation. For substrate specificity analysis, we tested the activities against 100 mM sucrose, maltose, trehalose, melezitose, cellobiose, raffinose, and lactose for 2 h. All assays were performed in three independent experiments to calculate the means and S.D.

Sequence and Structural Comparisons—The sequence of InvA was used in the BLAST search against the non-redundant protein sequences database. Several A/N-Inv homologues were input to multiple sequence alignment using the program MultAlin (66) and visualized by ESPript 3.0 (67). The DALI server (26) was used to search the homologous structures. The structures of tGA and YgjK, which have a high structural similarity, were superimposed against InvA using the Superpose program (68) of CCP4i program suite.

Author Contributions—J. X., H.-X. H., Y. C., and C.-Z. Z. designed the study. J. X., K. C., F. Y., and P.-F. H. performed the experiments. J. X., H.-X. H., Y.-L. J., D.-D. C., W. F. L., Y. C., and C.-Z. Z. analyzed the data. J. X., Y. C., and C.-Z. Z. wrote the paper.

Acknowledgments—We appreciate the assistance of the staff at the Shanghai Synchrotron Radiation Facility (SSRF) and the Core Facility Center for Life Sciences in University of Science and Technology of China. We are grateful to all of the developers of the CCP4 Suite, PyMOL, PHENIX, and ESPript.

References

1. Vargas, W. A., and Salerno, G. L. (2010) The Cinderella story of sucrose hydrolysis: alkaline/neutral invertases, from cyanobacteria to unforeseen roles in plant cytosol and organelles. *Plant Sci.* **178,** 1–8
2. Ruan, Y.-L., Jin, Y., Yang, Y.-J., Li, G.-J., and Boyer, J. S. (2010) Sugar input, metabolism, and signaling mediated by invertase: roles in development, yield potential, and response to drought and heat. *Mol. Plant* **3,** 942–955
3. Koch, K. (2004) Sucrose metabolism: regulatory mechanisms and pivotal roles in sugar sensing and plant development. *Curr. Opin. Plant Biol.* **7,** 235–246
4. Salerno, G. L., and Curatti, L. (2003) Origin of sucrose metabolism in higher plants: when, how, and why? *Trends Plant Sci.* **8,** 63–69
5. Ruan, Y.-L. (2014) Sucrose metabolism: gateway to diverse carbon use and sugar signaling. *Annu. Rev. Plant Biol.* **65,** 33–67
6. Coleman, H. D., Yan, J., and Mansfield, S. D. (2009) Sucrose synthase affects carbon partitioning to increase cellulose production and altered cell wall ultrastructure. *Proc. Natl. Acad. Sci. U.S.A.* **106,** 13118–13123
7. Barratt, D. H., Derbyshire, P., Findlay, K., Pike, M., Wellner, N., Lunn, J., Feil, R., Simpson, C., Maule, A. J., and Smith, A. M. (2009) Normal growth of *Arabidopsis* requires cytosolic invertase but not sucrose synthase. *Proc. Natl. Acad. Sci. U.S.A.* **106,** 13124–13129
8. Kolman, M. A., Nishi, C. N., Perez-Cenci, M., and Salerno, G. L. (2015) Sucrose in cyanobacteria: from a salt-response molecule to play a key role in nitrogen fixation. *Life* **5,** 102–126

9. Vargas, W. A., Nishi, C. N., Giarrocco, L. E., and Salerno, G. L. (2011) Differential roles of alkaline/neutral invertases in Nostoc sp. PCC 7120: Inv-B isoform is essential for diazotrophic growth. *Planta* **233,** 153–162
10. Vargas, W., Cumino, A., and Salerno, G. L. (2003) Cyanobacterial alkaline/neutral invertases: origin of sucrose hydrolysis in the plant cytosol? *Planta* **216,** 951–960
11. Sturm, A. (1999) Invertases. Primary structures, functions, and roles in plant development and sucrose partitioning. *Plant Physiol.* **121,** 1–8
12. Gallagher, J. A., and Pollock, C. J. (1998) Isolation and characterization of a cDNA clone from *Lolium temulentum* L. encoding for a sucrose hydrolytic enzyme which shows alkaline/neutral invertase activity. *J. Exp. Bot.* **49,** 789–795
13. Qi, X., Wu, Z., Li, J., Mo, X., Wu, S., Chu, J., and Wu, P. (2007) AtCYT-INV1, a neutral invertase, is involved in osmotic stress-induced inhibition on lateral root growth in *Arabidopsis*. *Plant Mol. Biol.* **64,** 575–587
14. Sturm, A., and Tang, G. Q. (1999) The sucrose-cleaving enzymes of plants are crucial for development, growth, and carbon partitioning. *Trends Plant Sci.* **4,** 401–407
15. Lammens, W., Le Roy, K., Van Laere, A., Rabijns, A., and Van den Ende, W. (2008) Crystal structures of *Arabidopsis thaliana* cell-wall invertase mutants in complex with sucrose. *J. Mol. Biol.* **377,** 378–385
16. Alberto, F., Jordi, E., Henrissat, B., and Czjzek, M. (2006) Crystal structure of inactivated *Thermotoga maritima* invertase in complex with the trisaccharide substrate raffinose. *Biochem. J.* **395,** 457–462
17. Alberto, F., Bignon, C., Sulzenbacher, G., Henrissat, B., and Czjzek, M. (2004) The three-dimensional structure of invertase (β-fructosidase) from *Thermotoga maritima* reveals a bimodular arrangement and an evolutionary relationship between retaining and inverting glycosidases. *J. Biol. Chem.* **279,** 18903–18910
18. Reddy, A., and Maley, F. (1996) Studies on identifying the catalytic role of Glu-204 in the active site of yeast invertase. *J. Biol. Chem.* **271,** 13953–13957
19. Lou, Y., Gou, J. Y., and Xue, H. W. (2007) PIP5K9, an *Arabidopsis* phosphatidylinositol monophosphate kinase, interacts with a cytosolic invertase to negatively regulate sugar-mediated root growth. *Plant Cell* **19,** 163–181
20. Welham, T., Pike, J., Horst, I., Flemetakis, E., Katinakis, P., Kaneko, T., Sato, S., Tabata, S., Perry, J., Parniske, M., and Wang, T. L. (2009) A cytosolic invertase is required for normal growth and cell development in the model legume, *Lotus japonicus*. *J. Exp. Bot.* **60,** 3353–3365
21. Jia, L., Zhang, B., Mao, C., Li, J., Wu, Y., Wu, P., and Wu, Z. (2008) OsCYT-INV1 for alkaline/neutral invertase is involved in root cell development and reproductivity in rice (*Oryza sativa* L.). *Planta* **228,** 51–59
22. Xiang, L., Le Roy, K., Bolouri-Moghaddam, M. R., Vanhaecke, M., Lammens, W., Rolland, F., and Van den Ende, W. (2011) Exploring the neutral invertase-oxidative stress defence connection in *Arabidopsis thaliana*. *J. Exp. Bot.* **62,** 3849–3862
23. Lin, C.-L., Lin, H.-C., Wang, A.-Y., and Sung, H.-Y. (1999) Purification and characterization of an alkaline invertase from shoots of etiolated rice seedlings. *New Phytol.* **142,** 427–434
24. Lee, H. S., and Sturm, A. (1996) Purification and characterization of neutral and alkaline invertase from carrot. *Plant Physiol.* **112,** 1513–1522
25. Krissinel, E., and Henrick, K. (2007) Inference of macromolecular assemblies from crystalline state. *J. Mol. Biol.* **372,** 774–797
26. Holm, L., and Rosenström, P. (2010) Dali server: conservation mapping in 3D. *Nucleic Acids Res.* **38,** W545–W549
27. Aleshin, A. E., Feng, P.-H., Honzatko, R. B., and Reilly, P. J. (2003) Crystal structure and evolution of a prokaryotic glucoamylase. *J. Mol. Biol.* **327,** 61–73
28. Kurakata, Y., Uechi, A., Yoshida, H., Kamitori, S., Sakano, Y., Nishikawa, A., and Tonozuka, T. (2008) Structural insights into the substrate specificity and function of *Escherichia coli* K12 YgjK, a glucosidase belonging to the glycoside hydrolase family 63. *J. Mol. Biol.* **381,** 116–128
29. Gibson, R. P., Gloster, T. M., Roberts, S., Warren, R. A., Storch de Gracia, I., García, A., Chiara, J. L., and Davies, G. J. (2007) Molecular basis for trehalase inhibition revealed by the structure of trehalase in complex with potent inhibitors. *Angew Chem. Int. Ed Engl.* **46,** 4115–4119
30. Hidaka, M., Honda, Y., Kitaoka, M., Nirasawa, S., Hayashi, K., Wakagi, T., Shoun, H., and Fushinobu, S. (2004) Chitobiose phosphorylase from *Vibrio proteolyticus*, a member of glycosyl transferase family 36, has a clan GH-L-like (α/α)6 barrel fold. *Structure* **12,** 937–947
31. Guérin, D. M., Lascombe, M.-B., Costabel, M., Souchon, H., Lamzin, V., Béguin, P., and Alzari, P. M. (2002) Atomic (0.94 Å) resolution structure of an inverting glycosidase in complex with substrate. *J. Mol. Biol.* **316,** 1061–1069
32. Guimarães, B. G., Souchon, H., Lytle, B. L., David Wu, J. H., and Alzari, P. M. (2002) The crystal structure and catalytic mechanism of cellobiohydrolase CelS, the major enzymatic component of the *Clostridium thermocellum* cellulosome. *J. Mol. Biol.* **320,** 587–596
33. Sturm, A., Hess, D., Lee, H. S., and Lienhard, S. (1999) Neutral invertase is a novel type of sucrose-cleaving enzyme. *Physiol. Plant* **107,** 159–165
34. Liu, C.-C., Huang, L.-C., Chang, C.-T., and Sung, H.-Y. (2006) Purification and characterization of soluble invertases from suspension-cultured bamboo (*Bambusa edulis*) cells. *Food Chem.* **96,** 621–631
35. Vargas, W. A., Pontis, H. G., and Salerno, G. L. (2007) Differential expression of alkaline and neutral invertases in response to environmental stresses: characterization of an alkaline isoform as a stress-response enzyme in wheat leaves. *Planta* **226,** 1535–1545
36. Masuda, H., Takahashi, T., and Sugawara, S. (1987) The occurrence and properties of alkaline invertase in mature roots of sugar beets. *Agric. Biol. Chem* **51,** 2309–2314
37. Alvaro-Benito, M., Polo, A., González, B., Fernández-Lobato, M., and Sanz-Aparicio, J. (2010) Structural and kinetic analysis of *Schwanniomyces occidentalis* invertase reveals a new oligomerization pattern and the role of its supplementary domain in substrate binding. *J. Biol. Chem.* **285,** 13930–13941
38. Masuda, H., Takahashi, T., and Sugawara, S. (1988) Acid and alkaline invertases in suspension cultures of sugar beet cells. *Plant Physiol.* **86,** 312–317
39. Kim, D., Park, S. Y., Chung, Y., Park, J., Lee, S., and Lee, T. K. (2010) Biochemical characterization of soluble acid and alkaline invertases from shoots of etiolated pea seedlings. *J. Integr. Plant Biol.* **52,** 536–548
40. Reca, I. B., Brutus, A., D'Avino, R., Villard, C., Bellincampi, D., and Giardina, T. (2008) Molecular cloning, expression and characterization of a novel apoplastic invertase inhibitor from tomato (*Solanum lycopersicum*) and its use to purify a vacuolar invertase. *Biochimie* **90,** 1611–1623
41. Wang, L. T., Wang, A. Y., Hsieh, C. W., Chen, C. Y., and Sung, H. Y. (2005) Vacuolar invertases in sweet potato: molecular cloning, characterization, and analysis of gene expression. *J. Agric. Food Chem.* **53,** 3672–3678
42. Hussain, A., Rashid, M. H., Perveen, R., and Ashraf, M. (2009) Purification, kinetic and thermodynamic characterization of soluble acid invertase from sugarcane (*Saccharum officinarum* L.). *Plant Physiol. Biochem.* **47,** 188–194
43. Omori, T., Ueno, K., Muramatsu, K., Kikuchi, M., Onodera, S., and Shiomi, N. (2010) Characterization of recombinant β-fructofuranosidase from *Bifidobacterium adolescentis* G1. *Chem. Cent. J.* **4,** 9
44. Chen, J. Q., and Black, C. C. (1992) Biochemical and immunological properties of alkaline invertase isolated from sprouting soybean hypocotyls. *Arch. Biochem. Biophys.* **295,** 61–69
45. Van den Ende, W., and Van Laere, A. (1995) Purification and properties of a neutral invertase from the roots of *Cichorium intybus*. *Physiol. Plant* **93,** 241–248
46. Liu, S., Lan, J., Zhou, B., Qin, Y., Zhou, Y., Xiao, X., Yang, J., Gou, J., Qi, J., Huang, Y., and Tang, C. (2015) HbNIN2, a cytosolic alkaline/neutral-invertase, is responsible for sucrose catabolism in rubber-producing laticifers of *Hevea brasiliensis* (para rubber tree). *New Phytol.* **206,** 709–725
47. Lombard, V., Golaconda Ramulu, H., Drula, E., Coutinho, P. M., and Henrissat, B. (2014) The carbohydrate-active enzymes database (CAZy) in 2013. *Nucleic Acids Res.* **42,** D490–D495
48. Schomburg, I., Chang, A., and Schomburg, D. (2002) BRENDA, enzyme data and metabolic information. *Nucleic Acids Res.* **30,** 47–49
49. Sim, L., Willemsma, C., Mohan, S., Naim, H. Y., Pinto, B. M., and Rose, D. R. (2010) Structural basis for substrate selectivity in human maltase-glucoamylase and sucrase-isomaltase N-terminal domains. *J. Biol. Chem.* **285,** 17763–17770

50. Hertel, S., Heinz, F., and Vogel, M. (2000) Hydrolysis of low-molecular-weight oligosaccharides and oligosaccharide alditols by pig intestinal sucrase/isomaltase and glucosidase/maltase. *Carbohydr. Res.* **326,** 264–276
51. Barker, M. K., and Rose, D. R. (2013) Specificity of processing α-glucosidase I is guided by the substrate conformation: crystallographic and *in silico* studies. *J. Biol. Chem.* **288,** 13563–13574
52. Hamazaki, H., and Hotta, K. (1980) Enzymatic hydrolysis of disaccharide unit of collagen: isolation of 2-*O*-α-D-glucopyranosyl-*O*-β-α-galactopyranosyl-hydroxylysine glucohydrolase from rat spleens. *Eur. J. Biochem.* **111,** 587–591
53. Mitsuishi, Y., Kobayashi, M., and Matsuda, K. (1980) Dextran α-(1 yields 2)-debranching enzyme from *Flavobacterium* sp. M-73: properties and mode of action. *Carbohydr. Res.* **83,** 303–313
54. Kim, H.-S., Park, H.-J., Heu, S., and Jung, J. (2004) Molecular and functional characterization of a unique sucrose hydrolase from *Xanthomonas axonopodis* pv. glycines. *J. Bacteriol.* **186,** 411–418
55. Kim, M.-I., Kim, H.-S., Jung, J., and Rhee, S. (2008) Crystal structures and mutagenesis of sucrose hydrolase from *Xanthomonas axonopodis* pv. glycines: insight into the exclusively hydrolytic amylosucrase fold. *J. Mol. Biol.* **380,** 636–647
56. Walden, H. (2010) Selenium incorporation using recombinant techniques. *Acta Crystallogr. D Biol. Crystallogr.* **66,** 352–357
57. Otwinowski, Z., and Minor, W. (1997) Processing of X-ray diffraction data collected in oscillation mode. *Methods Enzymol.* **276,** 307–326
58. Brodersen, D. E., de La Fortelle, E., Vonrhein, C., Bricogne, G., Nyborg, J., and Kjeldgaard, M. (2000) Applications of single-wavelength anomalous dispersion at high and atomic resolution. *Acta Crystallogr. D Biol. Crystallogr.* **56,** 431–441
59. Adams, P. D., Afonine, P. V., Bunkóczi, G., Chen, V. B., Davis, I. W., Echols, N., Headd, J. J., Hung, L.-W., Kapral, G. J., Grosse-Kunstleve, R. W., McCoy, A. J., Moriarty, N. W., Oeffner, R., Read, R. J., Richardson, D. C., Richardson, J. S., Terwilliger, T. C., and Zwart, P. H. (2010) PHENIX: a comprehensive Python-based system for macromolecular structure solution. *Acta Crystallogr. D Biol. Crystallogr.* **66,** 213–221
60. Murshudov, G. N., Skubák, P., Lebedev, A. A., Pannu, N. S., Steiner, R. A., Nicholls, R. A., Winn, M. D., Long, F., and Vagin, A. A. (2011) REFMAC5 for the refinement of macromolecular crystal structures. *Acta Crystallogr. D Biol. Crystallogr.* **67,** 355–367
61. Collaborative and Computational Project, Number 4. (1994) The CCP4 suite: programs for protein crystallography. *Acta Crystallogr. D Biol. Crystallogr.* **50,** 760–763
62. Emsley, P., and Cowtan, K. (2004) Coot: model-building tools for molecular graphics. *Acta Crystallogr. D Biol. Crystallogr.* **60,** 2126–2132
63. Vagin, A., and Teplyakov, A. (1997) MOLREP: an automated program for molecular replacement. *J. Appl. Crystallogr* **30,** 1022–1025
64. Afonine, P. V., Grosse-Kunstleve, R. W., Echols, N., Headd, J. J., Moriarty, N. W., Mustyakimov, M., Terwilliger, T. C., Urzhumtsev, A., Zwart, P. H., and Adams, P. D. (2012) Towards automated crystallographic structure refinement with phenix.refine. *Acta Crystallogr. D Biol. Crystallogr.* **68,** 352–367
65. Chen, V. B., Arendall, W. B., 3rd, Headd, J. J., Keedy, D. A., Immormino, R. M., Kapral, G. J., Murray, L. W., Richardson, J. S., and Richardson, D. C. (2010) MolProbity: all-atom structure validation for macromolecular crystallography. *Acta Crystallogr. D Biol. Crystallogr.* **66,** 12–21
66. Corpet, F. (1988) Multiple sequence alignment with hierarchical clustering. *Nucleic Acids Res.* **16,** 10881–10890
67. Robert, X., and Gouet, P. (2014) Deciphering key features in protein structures with the new ENDscript server. *Nucleic Acids Res.* **42,** W320–W324
68. Krissinel, E., and Henrick, K. (2004) Secondary-structure matching (SSM), a new tool for fast protein structure alignment in three dimensions. *Acta Crystallogr. D Biol. Crystallogr.* **60,** 2256–2268

Structural Analysis of the Catalytic Mechanism and Substrate Specificity of *Anabaena* Alkaline Invertase InvA Reveals a Novel Glucosidase

Jin Xie, Kun Cai, Hai-Xi Hu, Yong-Liang Jiang, Feng Yang, Peng-Fei Hu, Dong-Dong Cao, Wei-Fang Li, Yuxing Chen and Cong-Zhao Zhou

J. Biol. Chem. 2016, 291:25667-25677.
doi: 10.1074/jbc.M116.759290 originally published online October 24, 2016